A bistable microelectronic circuit for sensing extremely low electric field

Visarath In,[1,a)] Patrick Longhini,[1] Norman Liu,[1,b)] Andy Kho,[1] Joseph D. Neff,[1,c)] Antonio Palacios,[2,d)] and Adi R. Bulsara[1]
[1]*Space and Naval Warfare Systems Center Pacific, 53560 Hull Street, San Diego, California 92152-5001, USA*
[2]*Department of Mathematics and Statistics, Nonlinear Dynamics Group, San Diego State University, San Diego, California 92182, USA*

(Received 1 May 2009; accepted 12 November 2009; published online 6 January 2010)

Bistable systems are prevalently found in many sensor systems. Recently, we have explored (unidirectionally) coupled overdamped bistable systems that admit self-sustained oscillations when the coupling parameter is swept through the critical points of bifurcations [V. In *et al.*, Phys. Rev. E **68**, 045102(R) (2003); A. R. Bulsara *et al.*, Phys. Rev. E **70**, 036103 (2004); V. In *et al.*, Phys. Rev. E **72**, 045104(R) (2005); Phys Rev. Lett. **91**, 244101 (2003); A. Palacios *et al.*, Phys. Rev. E **72**, 026211 (2005); V. In *et al.*, Phys. Rev. E **73**, 066121 (2006)]. Complex behaviors emerge, in addition, from these (relatively simple) coupled systems when an external signal (ac or dc) is applied uniformly to all the elements in the array. In particular, we have demonstrated this emergent behavior for a coupled system comprised of mean-field hysteretic elements describing a "single-domain" ferromagnetic sample. The results are being used to develop extremely sensitive magnetic sensors capable of resolving field changes as low as 150 pT by observing the changes in the oscillation characteristics of the coupled sensors. In this paper, we explore the underlying dynamics of a coupled bistable system realized by coupling microelectronic circuits, which belong to the same class of dynamics as the aforementioned (ferromagnetic) system, with the nonlinear features and coupling terms modeled by hyperbolic tangent nonlinearities; these nonlinearities stem from the operational transconductance amplifiers used in constructing the microcircuits. The emergent behavior is being applied to develop an extremely sensitive electric-field sensor. © *2010 American Institute of Physics*. [doi:10.1063/1.3272052]

I. INTRODUCTION

It is well established that a well-designed coupling scheme, together with an appropriate choice of initial conditions, can induce oscillations (i.e., periodic switching between stable fixed points) in overdamped bistable dynamical systems when a control parameter exceeds a threshold value.[1–3] We have demonstrated this behavior in a specific prototype system comprised of three unidirectionally coupled ferromagnetic cores, the basis of a coupled core fluxgate magnetometer. Another prototypical (quartic potential based) system of coupled overdamped Duffing elements has been applied to describe the dynamics of the polarization inside a ferroelectric material,[3] the basis of an electric-field sensor, currently under development. Our analysis showed that N (*odd*) unidirectionally coupled elements with cyclic boundary conditions would oscillate when a control parameter, i.e., coupling strength, exceeded a critical value; note that the oscillatory behavior can also be seen for large, even N. Typically, the oscillations emerge with an infinite period through a heteroclinic-cycle bifurcation, i.e., a global bifurcation to a collection of solution trajectories that connects sequences of equilibria and/or periodic solutions. In the particular case of overdamped bistable systems, the cycle includes mainly saddle-node equilibria. As a control parameter (usually the coupling strength) approaches from above a critical value, the frequency of the oscillations decreases, approaching zero at the critical point. Past the critical value, the oscillations disappear, and the system dynamics settles into an equilibrium.

The basin of attraction of the oscillations spans almost the entire phase space with the exception of a small region near the symmetrical initial conditions; in which case, the coupled system settles asymptotically to its stable fixed points. The emergent oscillations, in either the ferromagnetic or ferroelectric systems mentioned above, have been used to detect very weak "target" (dc and ac) signals via the (signal-induced) changes in the oscillation characteristics, e.g., duty cycle and frequency. It is important to emphasize that this emergent oscillatory behavior is quite general; in a nonsensor application, it has led to interesting frequency-selective properties of interacting neural networks.[4,5]

The above phenomena open up new possibilities for the exploitation of a large class of (normally) nonoscillatory systems for a variety of practical applications that involve the use of the emergent self-sustained oscillations as a reference. The latest realization of a system in this class is an overdamped bistable system as one of the active elements in a microcircuit, which is intended to be used for measuring minute voltage or current changes that may be injected into the system. Details of the design, fabrication, and validation against theoretical work are all the subjects of this paper.

[a)]Electronic mail: visarath@spawar.navy.mil.
[b)]Electronic mail: norman@spawar.navy.mil.
[c)]Electronic mail: jdneff@spawar.navy.mil.
[d)]Electronic mail: palacios@euler.sdsu.edu.

Report Documentation Page

Form Approved
OMB No. 0704-0188

1. REPORT DATE	2. REPORT TYPE	3. DATES COVERED
MAY 2009		**00-00-2009 to 00-00-2009**

4. TITLE AND SUBTITLE	5a. CONTRACT NUMBER
A bistable microelectronic circuit for sensing extremely low electric field	5b. GRANT NUMBER
	5c. PROGRAM ELEMENT NUMBER
6. AUTHOR(S)	5d. PROJECT NUMBER
	5e. TASK NUMBER
	5f. WORK UNIT NUMBER
7. PERFORMING ORGANIZATION NAME(S) AND ADDRESS(ES) **Space and Naval Warfare Systems Center Pacific,53560 Hull Street,San Diego,CA,92152-5001**	8. PERFORMING ORGANIZATION REPORT NUMBER
9. SPONSORING/MONITORING AGENCY NAME(S) AND ADDRESS(ES)	10. SPONSOR/MONITOR'S ACRONYM(S)
	11. SPONSOR/MONITOR'S REPORT NUMBER(S)

12. DISTRIBUTION/AVAILABILITY STATEMENT
Approved for public release; distribution unlimited

13. SUPPLEMENTARY NOTES

14. ABSTRACT

15. SUBJECT TERMS

16. SECURITY CLASSIFICATION OF:			17. LIMITATION OF ABSTRACT	18. NUMBER OF PAGES	19a. NAME OF RESPONSIBLE PERSON
a. REPORT	b. ABSTRACT	c. THIS PAGE			
unclassified	**unclassified**	**unclassified**	**Same as Report (SAR)**	**8**	

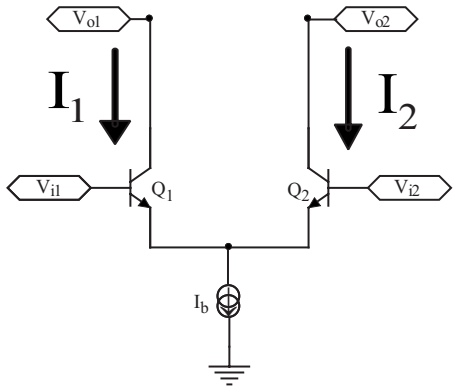

FIG. 1. The differential pair is used as the basic building block in the bistable elements. It consists of two transistors (Q_1 and Q_2) and a current source.

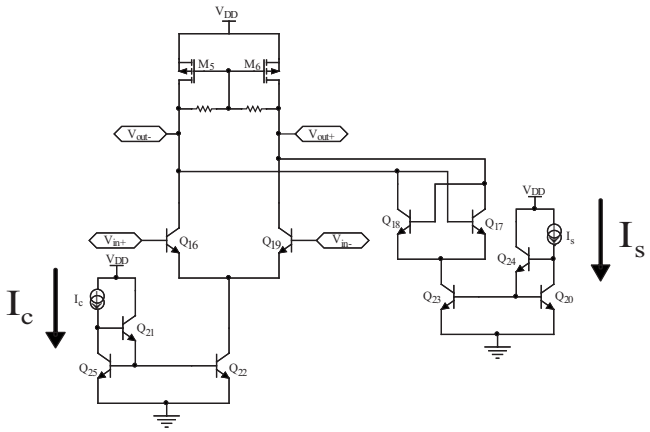

FIG. 2. A single (bistable) element is constructed out of differential pairs. Each element contains a cross coupled pair, input signal circuitry, and coupling components.

Section II presents a block-circuit diagram of the microcircuit and the derivation of the dynamical network equations. Section III includes the dynamical analysis, including the bifurcation properties in response to an input dc signal; we note that detection of ac signals is also possible; however, the ensuing behavior is quite intricate and rich, and will be described in future work. Section IV describes the microcircuit response to the (dc) input signal; the results obtained via numerical simulations as well as the experimental system are presented. Finally, in Sec. V, we present some concluding remarks and a discussion of (potential) future developments.

II. CIRCUIT AND DYNAMICAL EQUATIONS

The circuit implementation of each element in the system is based on differential pair designs composed of current mirrors to form the operational transconductance amplifiers (OTAs) that are responsible for the nonlinearity in the system. A typical differential pair circuit is shown in Fig. 1. We now, briefly, describe the derivation of the dynamics of the circuit.

The current and voltage relationship of a differential pair can be modeled[6] as

$$I_1 - I_2 = I_b \tanh[c(V_{i1} - V_{i2})], \tag{1}$$

where I_b is the bias (or tail) current of the differential pair and c is a device parameter that depends on temperature as well as on the fabrication process of the microelectronic circuit.

The schematic of a single element is shown in Fig. 2. It consists of two differential pairs that employ negative-positive-negative (NPN) transistors with one of them being cross coupled, two positive channel metal oxide semiconductor (PMOS) transistors, and a pair of resistors. In each differential pair, the current source in Fig. 1 is replaced with a current mirror. The two PMOS transistors are used as the load of the two differential pairs, and the two resistors are used for both the system dynamics and common-mode feedback. Since the circuit is fully differential (i.e., the outputs $V_{\text{out+}}$ and $V_{\text{out-}}$ are equal in magnitude but are out of phase by π), the common-mode voltages at $V_{\text{out+}}$ and $V_{\text{out-}}$ need to be "tracked" to take account of mismatches in the manufacture of the device; this is done by the resistor pairs, which "track" the voltages at these two nodes and can be adjusted to make sure that they are the same.

In order to input an external signal into the circuit, an input current mirror, see Fig. 3, is implemented on the overall system. The external signal (in this case an electric field that has been transduced into a current via an appropriate collection mechanism) I_{sig} is amplified using a NPN transistor and then the amplified signal is duplicated to output nodes (I_{01}, I_{o2}, and I_{o3}) using the current mirrors. By doing so, $I_{\text{out}} = \beta I_{\text{sig}}$, where β is the current gain of the NPN transistor. Finally, each output node is connected to node $V_{\text{out-}}$ (in Fig. 2) of each element.

Using nodal analysis, the current equations at the output nodes $V_{\text{out+}}$ and $V_{\text{out-}}$ (in Fig. 1) of the ith element are as follows:

$$C_L \dot{V}_{\text{out+}} = I_P + \frac{V_{g_p} - V_{\text{out+}}}{R} - \frac{I_c}{2}\tanh[c_c(V_{\text{in-}} - V_{\text{in+}})]$$

$$- \frac{I_s}{2}\tanh[c_s(V_{\text{out-}} - V_{\text{out+}})],$$

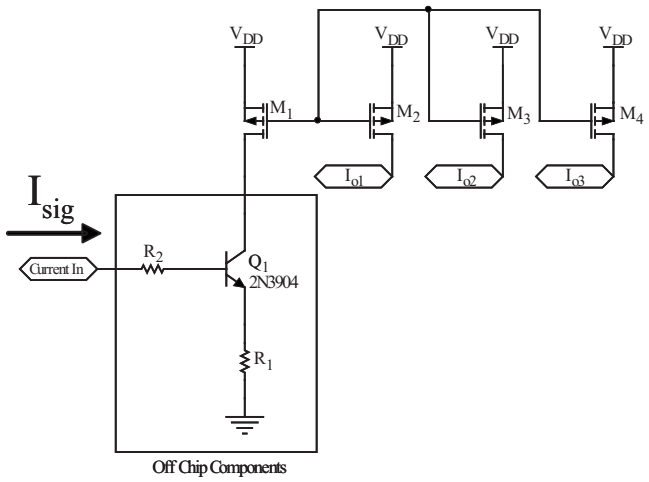

FIG. 3. The input current mirror provides the same current to each of the bistable elements of the coupled system shown in Fig. 4.

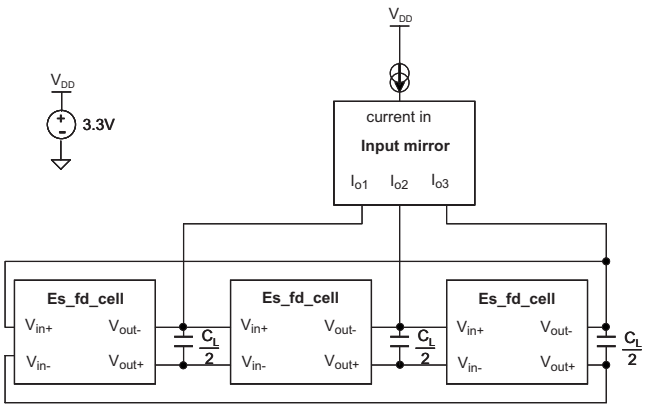

FIG. 4. Top-level schematic of a circuit realization of a coupled electric-field system with three units coupled unidirectionally.

$$C_L\dot{V}_{\text{out}-} = I_P + \frac{V_{g_p} - V_{\text{out}-}}{R} - \frac{I_c}{2}\tanh[c_c(V_{\text{in}+} - V_{\text{in}-})]$$

$$- \frac{I_s}{2}\tanh[c_s(V_{\text{out}+} - V_{\text{out}-})] + \varepsilon, \qquad (2)$$

where C_L is the load capacitance, R is the resistance of the pair of resistors in Fig. 2, c_c and c_s are the device parameters, which are proportional to $e/2kT$ and their values are approximately $(7-10)V^{-1}$, V_{g_p} is the gate voltage of the PMOS transistors in Fig. 2, V_{t_p} is a threshold voltage, I_p, which is equal to $-\mu_b C_{0x} W_p/2L_p(V_{DD}-V_{g_p}+V_{t_p})^2$, is the current through one of the PMOS transistors in Fig. 2, $V_{\text{in}+}$ and $V_{\text{in}-}$ are equal to the outputs $V_{\text{out}-}$ and $V_{\text{out}+}$ from the $(i-1)$th element, respectively, and we set $\varepsilon = \beta I_{\text{sig}}$. Note that ε corresponds to the external "target" signal, which has been transformed into a current I_{sig} that is then amplified by the NPN transistor. In fact, the circuit responds to very small (on the order of picoamperes) "source currents." Subtracting the bottom equation from the top equation in Eq. (2), we get the following expression:

$$C_L\dot{V}_i = -gV_i + I_s\tanh[c_sV_i] - I_c\tanh[c_cV_{i-1}] - \varepsilon, \qquad (3)$$

where $i=1,\ldots,3$, $V_0 \equiv V_3$, $V_i = V_{\text{out}+} - V_{\text{out}-}$ is the differential output of the ith element, and $g=1/R$. The top-level system schematic (for $N=3$) is shown in Fig. 4. The load circuit in the figure consists of a load capacitor with the value C_L connecting each node to ground. The value of C_L is chosen such that it is greater than the total parasitic capacitance C_P at that node (i.e., $C_L \gg 10C_P$). Equation (3) governs the underlying dynamics of a coupled bistable system realized by the microelectronic circuit of Fig. 4. The circuit and its dynamical description belong to the same class of bistable devices, as those of the ferromagnetic and ferroelectric systems studied theoretically in Refs. 1–3. Our aim is then to study the response of the (experimental) system to dc signals and validate that response against theoretical results. However, we would like to mention that subtle differences in the governing equations (mainly the characteristic function as well as the coupling term being described by a hyperbolic tangent function) lead to richer and more complex behavior in the response of the microcircuit to external ac signals, than what has been observed in our earlier theoretical models describing the coupled core magnetometer[2] and the ferroelectric capacitor based electric-field sensor.[3] This behavior will be described in a future publication.

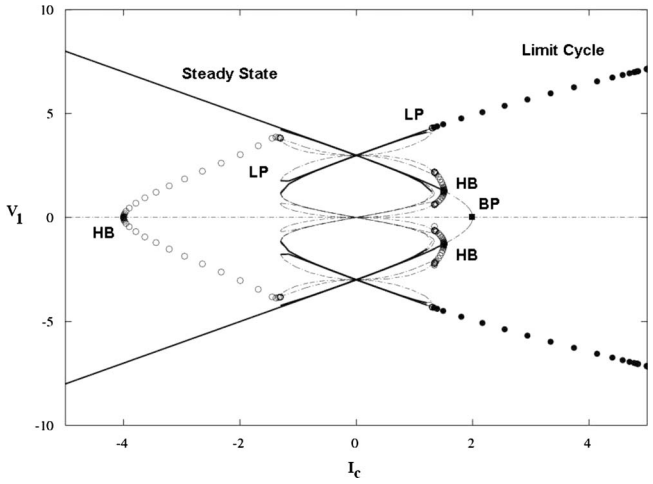

FIG. 5. Bifurcation diagram for a coupled ($N=3$) electric-field sensor microcircuit showing the system's voltage output in response to changes in coupling parameter I_c. The filled-in circles represent globally, asymptotically, stable limit-cycle oscillations created at the onset, LP, of a heteroclinic bifurcation. The solid lines depict the local branches of stable steady-state solutions. The empty circles correspond to unstable branches of periodic oscillations that emerge via Hopf bifurcations. The parameters are $C_L=1$, $g=1$, $c=1$, $I_s=2$ and $I_c=1$.

III. DYNAMICAL ANALYSIS

Equation (3) provides the starting point for a dynamical analysis aimed at chartering the different behavior that exists in various parameter regimes. In a coupled system such as this, one typically chooses an accessible system parameter that can be manipulated to force the system into a desired behavior. In this case the coupling coefficient I_c is used. Analogous to the procedure established in Ref. 1, the critical coupling coefficient can be calculated in closed form as

$$I_{c,\text{critical}} = \varepsilon - \frac{g}{c}\text{sech}^{-1}\left(\sqrt{\frac{g}{I_s c}}\right) + I_s\tanh\left[\text{sech}^{-1}\left(\sqrt{\frac{g}{I_s c}}\right)\right], \qquad (4)$$

where $c_s = c_c = c$ because the design of the OTAs for the nonlinearity and the coupling circuitries are assumed to be the same, for convenience. Here ε is assumed to be dc for this calculation; taking a time-periodic signal ε leads to an extremely rich behavior that is beyond the scope of the current work. Equation (4) is an analytical expression of the minimum coupling strength that is necessary for the coupled system to yield self-sustained oscillations. Mathematically speaking, it denotes the onset of the heteroclinic bifurcation, which is accompanied by the creation of the infinite-period (at the critical point) oscillations. This onset is the limit point, labeled LP, of the upper branch of limit-cycle oscillations shown in the one-parameter bifurcation diagram of Fig. 5.

We can readily observe the global nature of the heteroclinic bifurcation: At the birth point LP, the limit-cycle oscillations are fully grown with a well-defined amplitude as opposed to the local Hopf bifurcations, labeled HB, where the amplitude of the limit cycle increases as a square-root law of the distance from the bifurcation point. Observe also that all branches of Hopf bifurcations are unstable; hence they are marked with empty circles, while the global branch of limit cycles is marked with filled circles to indicate that it is stable. New branches of steady-state points or equilibria also emerge via local pitchfork bifurcations, labeled LP and BP. They are stable but their basin boundary of attraction is on the opposite side (with respect to the parameter I_c) of the global limit-cycle oscillations. The top-to-bottom symmetry of the bifurcation diagram is a direct consequence of the reflectional symmetry, i.e., $V_i \rightarrow \pm V_i$, inherent in governing equation (3). The diagram in Fig. 5 was generated computationally with the aid of the continuation software package AUTO.[7] Parameters were set to $\varepsilon=0$ and $C_L=1$ for ease of computations without worrying about time scales. In the circuit, C_L controls the overall response time of the collective coupled system, i.e., setting the upper boundary of the bandwidth of the coupled system. We would like to emphasize that the one-parameter bifurcation diagram for the circuit realization shown in Fig. 5 is in very good agreement with that of the theoretical analysis presented elsewhere.[3]

Consider, now, that the parameter I_s in Eq. (3) controls the bistability of the unit (uncoupled) cell. By varying this parameter, the unit cell's potential function can be monostable when $I_s < g/c_s$ and bistable for $I_s \geq g/c_s$. The potential function topology is similar to what has been seen in the soft-potential system describing the ferromagnetic materials employed in the fluxgate magnetometers.[1] To give a clearer picture of the separations between the oscillatory behavior and the nonoscillatory behavior, we perform a two-parameter bifurcation analysis to determine the boundaries, in parameter space (I_s, I_c), of the self-sustained limit-cycle oscillations. Figure 6 shows the resulting diagram as I_s and I_c are swept through their full ranges in the circuits. Note that we have chosen these parameters because they are, precisely, the accessible parameters in the systems that may be set by the designer/user for an appropriate desired behavior. More importantly, the diagram confirms the existence of an open region where the limit-cycle oscillations are globally asymptotically stable.

IV. NUMERICAL AND EXPERIMENTAL RESULTS

In order to operate the coupled bistable circuit to sense an input signal, e.g., signal gathered from an external collector such as an antenna or other similar implementation, an examination of the oscillation characteristics is typically employed once the system is tuned into the oscillation regime. The oscillation frequency depends on the external signal ε; it decreases with increasing signal strength. The other effect is that, assuming ε to be dc, the duty cycle of the oscillation is changed to being less than 50% with $\varepsilon \neq 0$. Figure 7 illustrates the effect of changing the external signal ε on the oscillations.

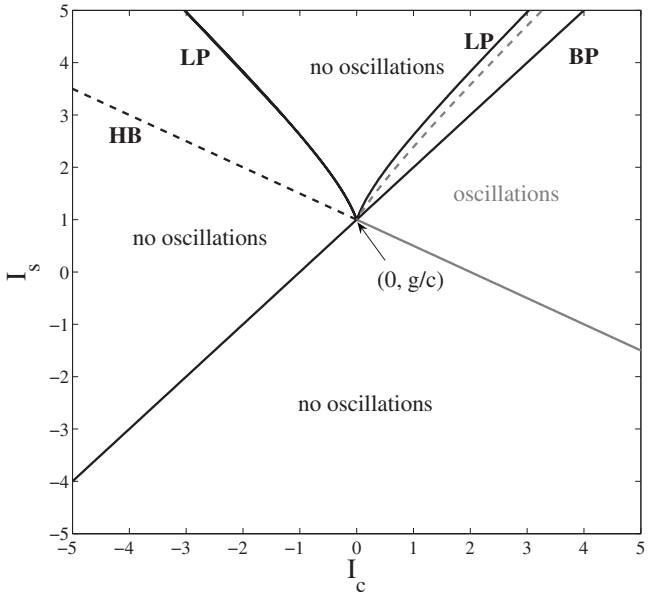

FIG. 6. Two-parameter bifurcation diagram for a coupled ($N=3$) electric-field system in parameter space (I_s, I_c). The diagram confirms the existence of an open region where limit-cycle oscillations are globally, asymptotically, stable. The diagram, as well as the stability properties of the solutions found in each region, was determined numerically using continuation software (Ref. 7). The dashed lines represent when the Hopf bifurcation becomes unstable. The parameters as in Fig. 5.

The rate at which the frequency decreases is governed by a power-$\frac{1}{2}$ law that is universal for this type of bifurcation, see Fig. 8. The frequency response shown in that figure was obtained through numerical simulations of model equation (3).

It has been shown in previous work that without the presence of an input signal, the differential output V_i should

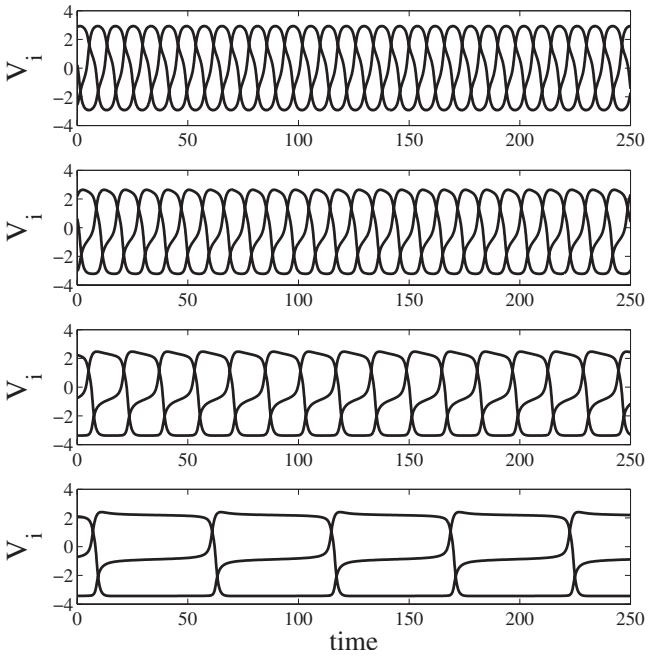

FIG. 7. Time series of oscillatory behavior in a coupled ($N=3$) electric-field system. As $\varepsilon=[0, 0.25, 0.4, 0.46]$ increases from the top panel to the bottom one, the frequency of the oscillations decreases correspondingly. The parameters as in Fig. 5.

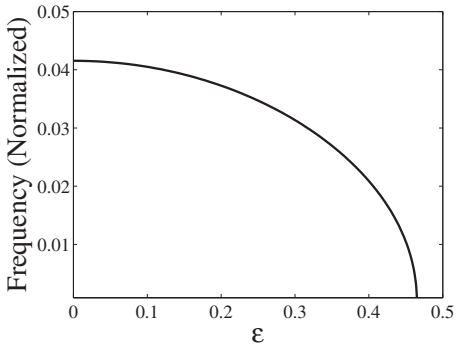

FIG. 8. Frequency response to the input signal ε for a coupled ($N=3$) electric-field sensor system, obtained from numerical simulations of model equation (3). The frequency scales by the universal power-$\frac{1}{2}$ law, which is typical for this type of bifurcation scenario. The parameters as in Fig. 5.

be symmetric in its duty cycle. That is, during a period of the output, the time above $V=0$, t_p, is the same as the time below $V=0$, t_n. The "residence times" t_p and t_n were introduced in Ref. 8, and the "residence time difference" RTD$=|t_p-t_n|$ should be zero in the absence of the external signal. As the input signal increases, the differential output becomes more asymmetric in its duty cycle, which results in an increase in RTD. Figure 9 shows this effect with increasing external field strength, obtained from numerical simulations of model equation (3). The slope of the RTD response curve is the sensitivity of the sensor. Note that as ε is increased, the response curve takes a very sharp upward turn past the value (obtained for the set of parameters used in this figure) of 0.4. This point is very near the critical point of bifurcation to the heteroclinic cycle. For sensor operation where detecting very weak signal change is desired, this is the optimal regime where one would tune the system to get the most sensitivity.[9]

In Sec. IV A, we present a rapid overview of the theoretical approach used to obtain analytic expressions for the oscillation period and the RTD. The calculation flows analogously to that described (albeit for a different dynamical system) in Ref. 1; hence we provide only its salient features in the current work.

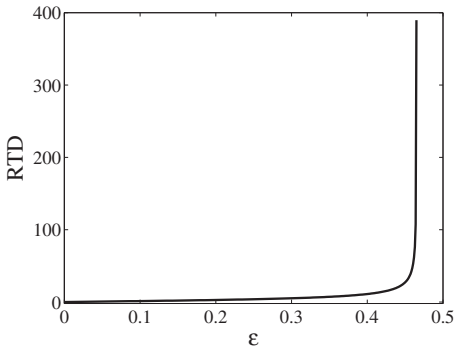

FIG. 9. RTD measures as a function of input signal strength ε, for a coupled ($N=3$) electric-field sensor system, obtained from numerical simulations of model equation (3). The sensitivity of the coupled sensor device is proportional to the slope of the RTD curve. Notice that the slope is particularly large near $\varepsilon=0.45$, which is near the bifurcation point that leads to oscillatory behavior in the device. The parameters as in Fig. 5.

A. Theoretical approach to calculate period and RTD response

We start with a scaled version of system (3) for $N=3$ as follows:

$$x_1' = -x_1 + I_s \tanh[dx_1] - I_c \tanh[dx_3] - \varepsilon,$$

$$x_2' = -x_2 + I_s \tanh[dx_2] - I_c \tanh[dx_1] - \varepsilon,$$

$$x_3' = -x_3 + I_s \tanh[dx_3] - I_c \tanh[dx_2] - \varepsilon, \tag{5}$$

with the change in variables $x_i=gV_i$ and scaling time by $\tau=g/C_L$, so that differentiation $(\,)'$ in Eq. (5) is with respect to τ. Note that $d=c/g$. In the absence of coupling, each element describes a particle in a bistable potential that has been asymmetrized through the addition of the target signal ε. Note that the signal ε is taken to be far smaller than the energy barrier height for the potential function corresponding to any (uncoupled) element. Then, one can compute the condition for bistability as $I_s c/g>1$. As already described in Ref. 1, we exploit the fact that the elements $x_{1,2,3}$ cross the energy barrier separating the stable steady states of their (uncoupled) potential *sequentially* with two elements remaining approximately confined to their steady states while the third (active) element switches; this is, readily, apparent in Fig. 7. This allows us to decouple the system with the active element described by a simple particle in a bistable potential framework, and the coupling term replaced with a constant term in the dynamics. Then, the problem boils down to computing the times t_1 and t_2 at which a particular element crosses the energy barrier (these times are unequal because the potential is asymmetric as a result of the signal term).

As an example, we consider the x_2 element, which is backcoupled to element x_1. Assuming x_1 to remain "frozen" at its stable minimum value x_{1m}, the x_2 equation reduces to

$$x_2' = f(x_2) \equiv -\frac{\partial U(x_2)}{\partial x_2}, \tag{6}$$

with the definitions

$$f(x_2) = -x_2 + I_s \tanh[dx_2] - \Delta_2,$$

$$\Delta_2 = I_c \tanh[dx_{1m}] + \varepsilon. \tag{7}$$

$U(x_2)$ is the potential energy function corresponding to the dynamics x_2' as set out in Eq. (6). Then, assuming the variable x_2 to be in its steady state x_{2m} (the left, or negative potential well) at time $t=0$, the time t_2 taken to cross the energy barrier and arrive in the opposite minimum x_{2p} is given by

$$t_2 = \int_{x_{2m}}^{0} \frac{dx_2}{f(x_2)}, \tag{8}$$

it being assumed that once the state point has crossed the energy barrier, it requires a negligible amount of time to "roll" down the energy slope into the (opposite) minimum. The integral is evaluated by realizing that $f(x_2)$ is peaked at $x_2=\tilde{x}_2$; this value is found by setting the derivative of $f(x_2)$ to zero and is given by $\tanh[d\tilde{x}_2]=\sqrt{(dI_s-1)/dIs}\equiv\alpha$. Simultaneously we note that, at $x_2=\tilde{x}_2$ and $I_c=I_{2cc}$, an inflexion point

will develop in the potential, as the state point switches from left to right. The condition for the point of inflexion [in the potential $U(x_2)$] leads to

$$\Delta_{2c} = I_{2cc}\tanh[dx_{1m}] + \varepsilon = -\tilde{x}_2 + I_s\tanh[d\tilde{x}_2], \tag{9}$$

so that we are led to the critical value of I_c to effect a switch from left to right in the potential function

$$I_{2cc} = (d^{-1}\,\text{arctanh}[\alpha] - I_s\alpha - \varepsilon)\coth[dx_{1m}]. \tag{10}$$

Finally, we take the expansion of $f(x_2)$ up to second order and write the integral in Eq. (8) as

$$t_2 \approx \int_{x_{2m}}^{0} \frac{dx_2}{\Delta_{2c} - \Delta_2 + \alpha(x_2 - \tilde{x}_2)^2}. \tag{11}$$

The integration limits may now be extended to $\pm\infty$ and the integral readily evaluated to yield

$$t_2 = \frac{\pi}{\sqrt{\alpha(\Delta_{2c} - \Delta_2)}}. \tag{12}$$

An analogous procedure yields the time t_1 required to make a switch in the opposite direction. The result is

$$t_1 = \frac{\pi}{\sqrt{\alpha(\Delta_1 - \Delta_{1c})}}, \tag{13}$$

with the critical coupling strength necessary in this case given by

$$I_{1cc} = (-d^{-1}\,\text{arctanh}[\alpha] + I_s\alpha - \varepsilon)\coth[dx_{1p}], \tag{14}$$

with x_{1p} denoting the location of the positive fixed point of the potential. Both x_{1p} and its negative counterpart x_{1m} may be computed via a perturbation expansion (assuming small ε); for brevity, we do not give the expressions here. It is most important to note that, in practice, to achieve reliable switching back and forth across the barrier, the coupling strength I_c in system (5) should be set to a value larger than the greater of (I_{1cc}, I_{2cc}).

We may now write down, analogous to the procedure followed in Ref. 1, the expressions for the oscillation period $T=3(t_1+t_2)$ and the RTD$=|t_1-t_2|$ as follows:

$$T = \frac{3\pi}{\sqrt{\alpha}}\left[\frac{1}{\sqrt{(I_{2cc} - I_c)\tanh[dx_{1m}]}} + \frac{1}{\sqrt{(I_c - I_{1cc})\tanh[dx_{1p}]}}\right] \tag{15}$$

and

$$\text{RTD} = \left|\frac{\pi}{\sqrt{\alpha}}\left[\frac{1}{\sqrt{(I_{2cc} - I_c)\tanh[dx_{1m}]}} - \frac{1}{\sqrt{(I_c - I_{1cc})\tanh[dx_{1p}]}}\right]\right| \tag{16}$$

with the characteristic scaling with respect to the square root of the "bifurcation distances" $|I_{2cc}-I_c|$ and $|I_{1cc}-I_c|$ readily apparent. We note that the signal (ε) induced asymmetry enters the above expressions through the critical values of the coupling coefficients; for $\varepsilon=0$ we obtain $t_1=t_2$ and the RTD vanishes, as expected. We must note, in passing, that theoretical expressions (15) and (16) provide the correct qualitative behavior for the period and RTD; they do not provide, however, an exact quantitative match. This is because our approximations to the integrals for $t_{1,2}$ do not work as well with the system at hand, as in the previously studied case of the coupled core magnetometer[1] because the coupling term (which modifies the potential topology) is outside the tanh function that describes the self-coupling behavior. A systematic error is introduced into the expression for the period; however, expression (16) does provide a good approximation, as is shown in Fig. 10, to the simulated value of the RTD because the errors in $t_{1,2}$ tend to nullify each other in the subtraction.

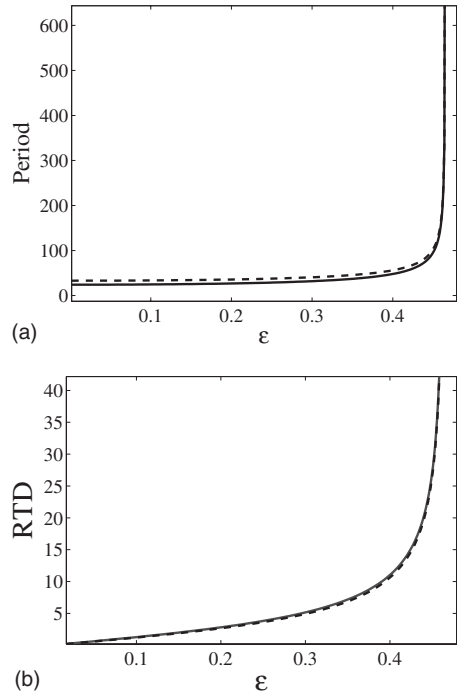

FIG. 10. Comparison of analytical approximations with numerical simulations for (top) period T and (bottom) RTD responses for a coupled electric-field sensor. The solid line indicates analytical approximations obtained through Eqs. (15) and (16), respectively. The dashed lines correspond to numerical results from simulations of hardware dynamics (3).

B. SPICE simulations and experiments

The design of the coupled bistable circuit has been simulated in SPICE where the parameters are set to $I_c=200\ \mu$A, $I_s=300\ \mu$A, $C_L=66$ nF, $R=500\ \Omega$, and $\beta=150$. The oscillation characteristics, Fig. 11, are similar to those results found using the mathematical model illustrated in Fig. 7. This serves to confirm the accuracy of the model and its design/implementation.

The experimental system is based on a fabricated device that follows the design provided by this manuscript. The load capacitance C_L is set to 66 nF, $I_c=200\ \mu$A, $I_s=300\ \mu$A, and $R=500\ \Omega$. The supplied voltage is 3.3 V to power the microcircuit. A source measure unit is used to inject the current I_{sig} into the bistable microcircuit to mimic the sensing current that would have appeared from the (in this case, electric charge) collecting apparatus. Figure 12 shows the response characteristics of the oscillation frequency and the measured RTD to the input signal I_{sig}; through an inspection of the

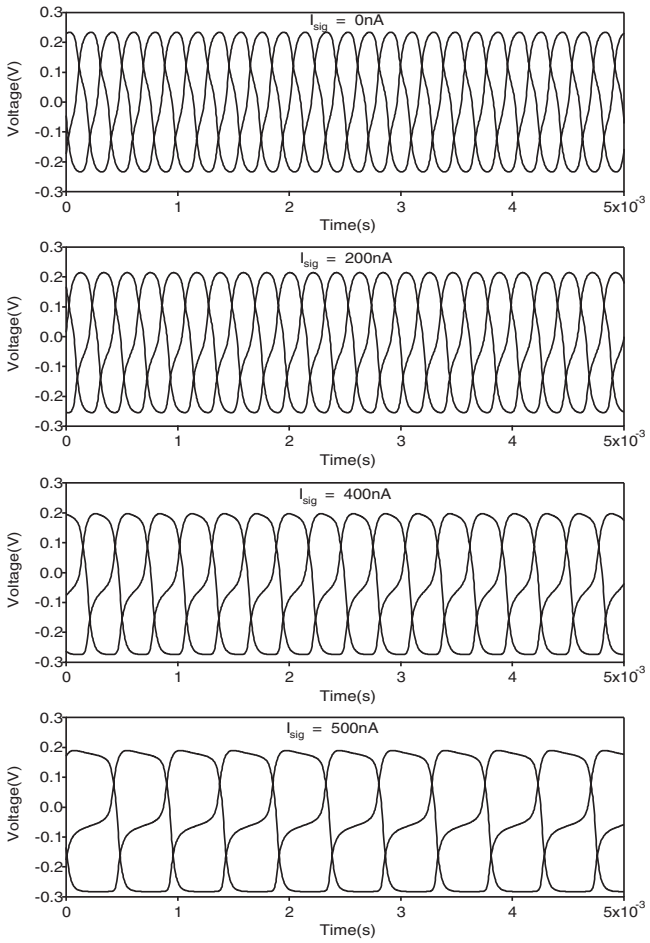

FIG. 11. Waveforms of the differential output from all three coupled elements, from a coupled electric-field sensor device, are plotted for different values of input dc I_{sig}. The outputs are characteristically out of phase by $2\pi/N(N=3)$ degrees, so that collectively they form a traveling wave pattern. From top to bottom, I_{sig} is set to 0, 200, 400, and 500 nA, respectively.

results, β is determined to be, approximately, 150. The experimental data confirm the results of the simulation of the theoretical model and the SPICE simulation of the design in Figs. 8, 9, and 13, respectively. In the current version of the experiment, the injected current cannot exceed 530 nA to avoid overloading the microcircuit. Steps are taken to increase the injected current range to push the system closer toward the bifurcation or to set the I_c parameter closer toward the bifurcation so that the RTD response curve is much closer to what is seen in the SPICE simulation of the design and the model, but for an ultrasensitive sensor, this is not the goal. The goal is to discern a very small current, which would translate into detecting a very small electric-field change. Figure 14 shows the time series from the experiment with various applied currents. As seen in the plots, there are some mismatches in the waveforms among the three outputs of the oscillators. These mismatches can be attributed to the circuit components, mainly the transistors that make up the OTAs. Future designs will attempt to minimize these component mismatch issues but they are not trivial.

V. CONCLUSION

We have presented a microelectronic circuit realization of a coupled bistable system suitable for detection of weak

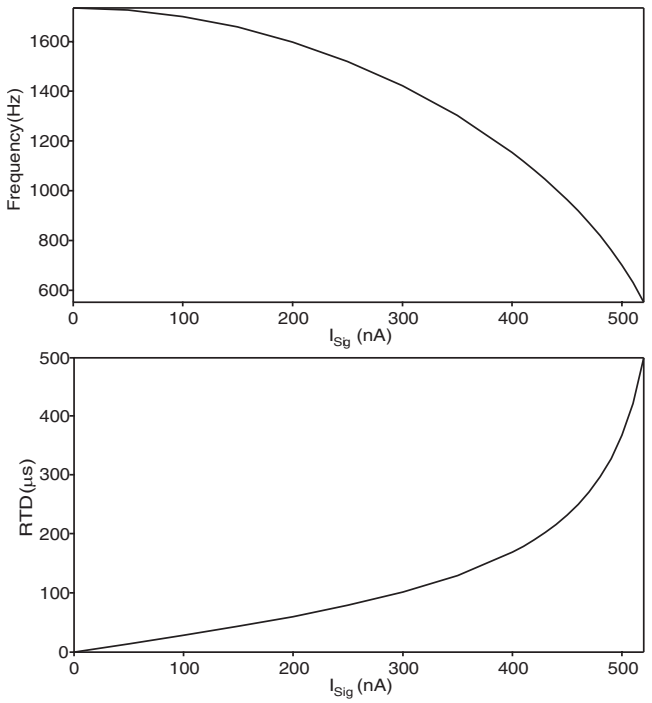

FIG. 12. Frequency and RTD responses of the experimental coupled electric-field sensor system subject to an injected current I_{sig}. The scaling factor (gain) β of the injected current is determined to be approximately 150. Observe the similarity between these two experimental responses and the numerical responses of model equation (3) shown previously in Figs. 8 and 9, respectively.

dc and ac signals (the case of ac signal detection is relegated to a forthcoming paper). The governing equations of the microcircuit are somewhat more complicated than those described in our earlier work on coupled dynamic ferromag-

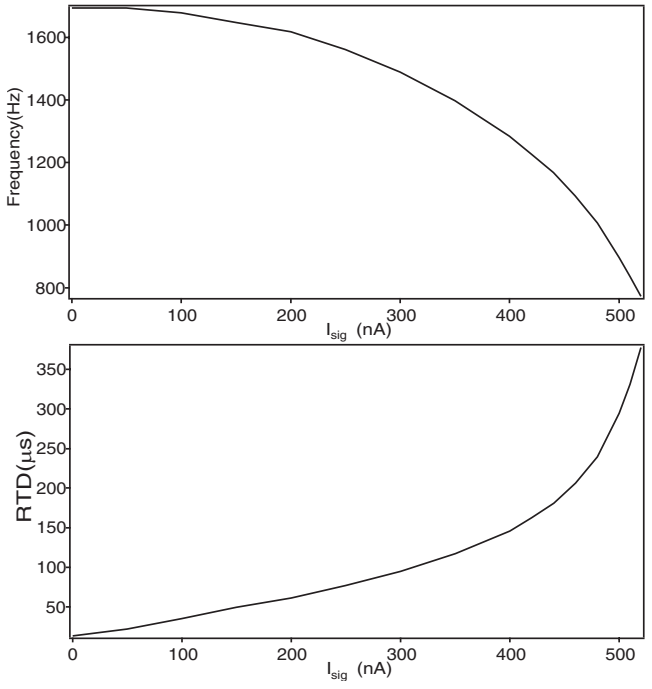

FIG. 13. Frequency and RTD responses of hardware simulations, via SPICE, of a coupled electric-field sensor. Observe the similarity between these two hardware-simulated responses of the design and the numerical responses of model equation (3) shown previously in Figs. 8 and 9, respectively.

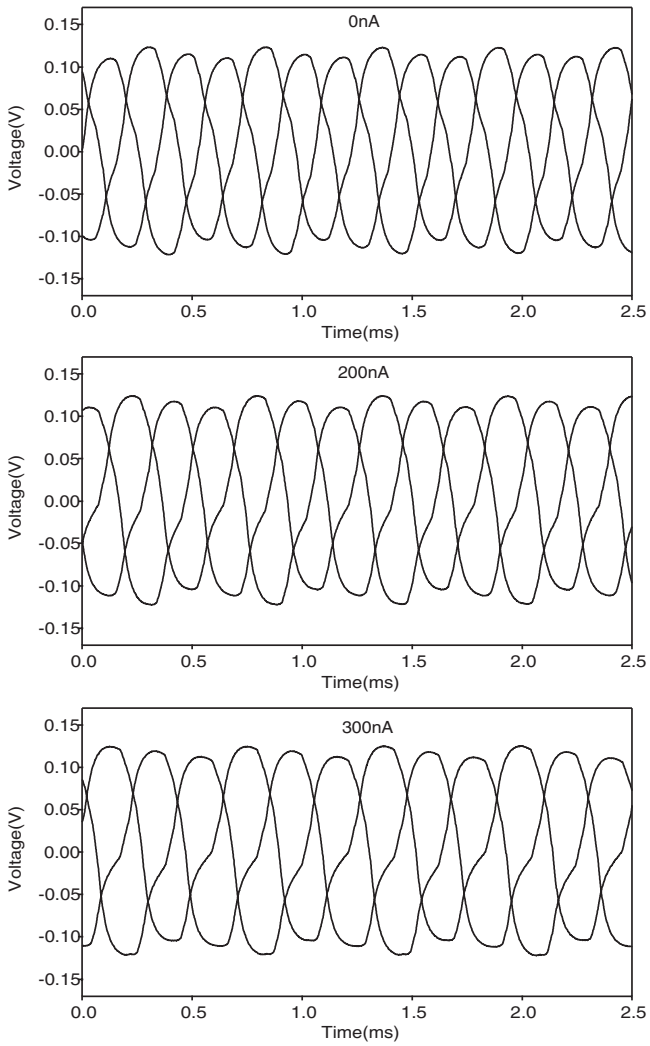

FIG. 14. Time series from the experimental system. Each graph shows the three waveforms from the three oscillators used in the coupled network. The first graph (top) shows the oscillations with zero applied current. The second graph is for applied current $I_{sig}=200$ nA. The third graph (bottom) is for the applied current $I_{sig}=300$ nA.

netic and ferroelectric elements. However, the behavior of the coupled system is, qualitatively, quite similar in all these cases; namely, the sensors all operate on the basis of self-sustained oscillations induced by the network topology, in particular, the coupling function. In all three systems, a bifurcation analysis shows that the oscillations emerge as a branch of limit-cycle oscillations that stems from a heteroclinic bifurcation connecting sequences of saddle-node steady states. The bifurcation is global, so at the bifurcation point the oscillations are fully grown but, more importantly, they emerge with an infinite period, at the critical point. The period is particularly important because a large period of oscillation can render the waveform highly sensitive to the detection of external dc/ac signals. We have exploited this feature in the implementation of the microcircuit device with a new readout mechanism, based on the RTD. The RTD mechanism relies on measuring the asymmetry of the waveform. In the absence of an external signal, the oscillations are top-to-bottom symmetric so there is no difference and hence no signal is detected. In the presence of a weak signal, however, an oscillation with a large period can yield a very large asymmetry and so the signal can be detected by measuring the difference.

Overall, the analysis and results of the microcircuit dynamics are in very good agreement with previous theoretical results. There are, however, important differences in the characteristic function and coupling function of the microcircuit device that can lead to far richer and more complex behavior in the detection of ac signals than in the theoretical models. For instance, additional branches of steady states and the possibility of chaotic behavior in the microcircuit are possible. A study of those differences is beyond the scope of the present paper but they will be addressed in future work.

The aim of this work was twofold. First to demonstrate that a circuit realization of theoretical models is feasible and, second, that there is a region of parameter space where the circuit dynamics, and its response to weak external dc signals, are in very good agreement with theory. In particular, we reiterate that the current work describes a microelectronic circuit that is highly sensitive to very small changes (e.g., stemming from small changes in the ambient electric field) in the input current. We defer the analysis of additional regimes in the microcircuit and its response to noise, to future work.

ACKNOWLEDGMENTS

The authors acknowledge the support from the Office of Naval Research (Code No. 30). A.P. was supported in part by the National Science Foundation Grant Nos. CMS-0625427 and CMS-0638814.

[1]V. In, A. R. Bulsara, A. Palacios, P. Longhini, A. Kho, and J. D. Neff, Phys. Rev. E **68**, 045102(R) (2003); A. R. Bulsara, V. In, A. Kho, W. J. Rappel, J. Acebron, A. Palacios, P. Longhini, S. Baglio, and B. Ando, *ibid.* **70**, 036103 (2004).
[2]V. In, A. R. Bulsara, A. Kho, P. Longhini, and A. Palacios, Phys. Rev. E **72**, 045104(R) (2005).
[3]V. In, A. Palacios, A. R. Bulsara, P. Longhini, A. Kho, J. D. Neff, S. Baglio, and B. Ando, Phys. Rev. E **73**, 066121 (2006).
[4]V. In, A. Kho, A. Palacios, P. Longhini, J. D. Neff, and B. K. Meadows, Phys. Rev. Lett. **91**, 244101 (2003).
[5]A. Palacios, R. Carretero-Gonzales, P. Longhini, N. Renz, V. In, A. Kho, J. Neff, B. K. Meadows, and A. R. Bulsara, Phys. Rev. E **72**, 026211 (2005).
[6]P. Gray, P. Hurst, S. Lewis, and R. Meyer, *Analysis and Design of Analog Integrated Circuits*, 4th ed. (Wiley, New York, 2001), pp. 215–217.
[7]E. Doedel and X. Wang, "Auto94: Software for continuation and bifurcation problems in ordinary differential equations," Applied Mathematics Report No. CRPC-TR94592, July 1994.
[8]A. R. Bulsara, C. Seberino, L. Gammaitoni, M. F. Karlsson, B. Lundqvist, and J. W. C. Robinson, Phys. Rev. E **67**, 016120 (2003).
[9]S. T. Vohra, L. Fabiny, and K. Wiesenfeld, Phys. Rev. Lett. **72**, 1333 (1994); S. T. Vohra and K. Wiesenfeld, Physica D **86**, 27 (1995); A. R. Bulsara, J. F. Lindner, V. In, A. Kho, S. Baglio, V. Sacco, B. Ando, P. Longhini, A. Palacios, and W. -J. Rappel, Phys. Lett. A **353**, 4 (2006); A. R. Bulsara, V. In, A. Kho, A. Palacios, P. Longhini, J. Neff, G. Anderson, C. Obra, S. Baglio and B. Ando, Meas. Sci. Tech. **19**, 075203 (2008).